

## PAPER



Cite this: *Dalton Trans.*, 2018, **47**, 9014

## Enhanced acetone sensing performance of Au nanoparticle modified porous tube-like ZnO derived from rod-like ZIF-L†

Huifen Fu,<sup>a</sup> Xun Wang,<sup>a</sup> Peng Wang,<sup>a</sup> Zhihua Wang,<sup>\*b</sup> Hang Ren<sup>a</sup> and Chong-Chen Wang<sup>†\*</sup>

Metal oxide semiconductors with a porous hollow structure have received great attention in many fields. In this work, a facile preparation method of porous tube-like ZnO (PT-ZnO) was developed by annealing rod-like ZIF-L at high temperature, and the formation mechanism of the tube-like structure was discussed in detail. The corresponding gas sensing performances were determined adopting acetone as the target gas. Gas-sensing test results show that PT-ZnO has better acetone sensing performance than that of porous plate-like ZnO (PP-ZnO) derived from leaf-like ZIF-L, resulting from the unique tube-like structure and larger amount of adsorbed oxygen. It is found that the introduction of Au nanoparticles greatly improves the acetone sensing performance, which can be attributed to the activation of acetone by Au and the increased amount of adsorbed oxygen. Au/PT-ZnO has the largest amount of adsorbed oxygen which even becomes the dominant oxygen species on the surface of PT-ZnO, resulting in the best acetone-sensing performance.

Received 31st May 2018,  
Accepted 13th June 2018

DOI: 10.1039/c8dt02219d

rsc.li/dalton

## Introduction

ZnO, as an n-type semiconductor, was widely used in gas sensors because of its low cost, nontoxic nature, good tunability, and so on.<sup>1–4</sup> However, the gas-sensing performance of ZnO is also required to be further improved to satisfy the practical applications. The sensing mechanism of the ZnO sensors follows the surface-controlled type,<sup>5,6</sup> in which the detected gases diffuse and are adsorbed on the surface of ZnO, and then react with the superficial active oxygen species, leading to the resistance change of ZnO. The porous hollow structure with abundant pores can facilitate the diffusion of targeted gases to improve its gas-sensing properties.<sup>7–12</sup> Lu's group prepared Au@ZnO yolk-shell nanospheres using carbon templates, and Au@ZnO responded well to acetone.<sup>8</sup> Han synthesized ZnO hollow spheres using a polystyrene sphere

template, which showed a high response to *n*-butanol because the hollow structure increased the specific surface areas and oxygen species.<sup>13</sup> Currently, porous hollow materials have received increasing interest in the field of gas sensors.<sup>14–16</sup> The hard-template method has been always used to prepare hollow materials, such as carbon and silica templates. However, this synthesis technique is complicated and time-consuming.<sup>17–21</sup>

Recently, metal-organic frameworks (MOFs) have received considerable attention in many fields because of their ultra-high surface areas, well ordered porous structures and structure designability.<sup>22–24</sup> As a kind of typical MOF, zeolitic imidazolate frameworks (ZIFs) constructed from tetrahedral metal ions like Zn<sup>2+</sup> or Co<sup>2+</sup> bridged by an imidazolate ligand have been widely studied in catalysis,<sup>25–27</sup> adsorption,<sup>28</sup> gas separation,<sup>29,30</sup> gas storage<sup>31–33</sup> and CO<sub>2</sub> capture,<sup>34</sup> due to their ultra-high surface area, permanent porosity with uniform pore cavity size and active metal sites.<sup>35,36</sup> Zhang reported for the first time that ZIF-67 had a good response to formaldehyde.<sup>37</sup> However, the poor electroconductivity of ZIFs limits their applications in the sensing field. Subsequently, Koo prepared PdO/Co<sub>3</sub>O<sub>4</sub> hollow nanocages from Pd@ZIF-67 *via* calcination, which exhibited good response and high selectivity to acetone.<sup>38</sup> Also, Li reported that hollow ZnO cubes obtained from the calcination of ZIF-8 responded well to benzene.<sup>39</sup>

Nowadays, numerous volatile organic compounds (VOCs) are discharged in air with the development of society and

<sup>a</sup>Beijing Key Laboratory of Functional Materials for Building Structure and Environment Remediation, Beijing University of Civil Engineering and Architecture, Beijing 100044, China. E-mail: chongchenwang@126.com

<sup>b</sup>State Key Laboratory of Chemical Resource, Beijing University of Chemical Technology, Beijing 100029, China. E-mail: zhwang@mail.buct.edu.cn

† Electronic supplementary information (ESI) available: Comparison of acetone-sensing performance, response time and recovery time, relative amount of oxygen species calculated from O 1s XPS. See DOI: 10.1039/c8dt02219d

especially the industry, which are harmful to human health. Gas sensors to detect the gaseous pollutants in air or even indoor air are important. Acetone is not only a kind of VOC but also a breath biomarker of patients with diabetes.<sup>40</sup> However, the low response and selectivity hinder the practical applications of acetone sensors. From this point, improving the acetone-sensing performance is urgent.

Most recently, our group unprecedentedly developed a facile method to prepare rod-like ZIF-L induced by polyvinylpyrrolidone (PVP),<sup>41</sup> which encouraged us to investigate the potential application of special rod-like ZIF-L. Within this paper, porous tube-like ZnO (PT-ZnO) was prepared easily from rod-like ZIF-L by calcination at 500 °C. It is found that the response of PT-ZnO toward acetone is higher than that of the porous plate-like ZnO (PP-ZnO) derived from leaf-like ZIF-L. In addition, the acetone sensing performance was further improved after the loading of Au NPs.

## Experimental

### Materials and instruments

Zn(NO<sub>3</sub>)<sub>2</sub> and 2-methylimidazole (2-MI) were purchased from J&K Scientific Ltd. Poly(vinyl pyrrolidone) (PVP K30) was purchased from Beijing Yili Fine Chemical Research Institute (Beijing, China). Chloroauric acid (HAuCl<sub>4</sub>·4H<sub>2</sub>O) and NaBH<sub>4</sub> were purchased from Sinopharm Chemical Reagent Co., Ltd (Shanghai, China). A Hitachi HT7700 transmission electron microscope (TEM) and a Hitachi S-4700 scanning electron microscope (SEM) were used to characterize the morphology of the samples. Powder X-ray diffraction (PXRD) patterns were recorded on a Dandonghaoyuan DX-2700B diffractometer using Cu K $\alpha$  radiation. Thermogravimetric analysis (TGA) was carried out on a DTU-3c thermal analyser. X-ray photoelectron spectra (XPS) were recorded using a VG Scientific ESCALAB 250 spectrometer. Nitrogen adsorption-desorption isotherms, pore size distributions and specific surface areas of these samples were obtained using a Belsorp II analyzer at liquid N<sub>2</sub> temperature (77 K). The loading of Au was measured by ICP-OES (Thermo Scientific iCAP 7200).

### Preparation of leaf-like ZIF-L

Leaf-like ZIF-L was prepared following a previously reported method with a slight modification.<sup>42</sup> 10 mmol 2-MI and 1 mmol Zn(NO<sub>3</sub>)<sub>2</sub> were each dissolved in 5 mL deionized water and then the two aqueous solutions were added in 50 mL deionized water in turn. After stirring evenly, this solution was held for 24 hours. Finally leaf-like ZIF-L was obtained after being centrifuged, washed with ethanol and dried in a drying oven at 60 °C.

### Preparation of rod-like ZIF-L

The preparation of rod-like ZIF-L was similar to that of leaf-like ZIF-L except that 0.25 g PVP was dissolved in 50 mL deionized water before 2-MI and Zn(NO<sub>3</sub>)<sub>2</sub> were added.

### Preparation of porous plate-like and tube-like ZnO

Leaf-like or rod-like ZIF-L were heated from room temperature to 500 °C at an increase rate of 1 °C min<sup>-1</sup>, and maintained at 500 °C for 30 min using a pipe furnace. After cooling down to room temperature, porous plate-like ZnO (PP-ZnO) or porous tube-like ZnO (PT-ZnO) were obtained.

### Preparation of Au/PT-ZnO and Au/PP-ZnO

0.1 g PP-ZnO (PT-ZnO) was dispersed in 20 mL deionized water, and 0.5 mL 4 g L<sup>-1</sup> HAuCl<sub>4</sub> was added in. Then 0.5 mL 100 mM NaBH<sub>4</sub> was injected into the above solution quickly. After 2 h, Au/PT-ZnO (Au/PT-ZnO) was obtained after being centrifuged, washed twice with ethanol, and dried in a dry oven. The loading of Au measured by ICP in the Au/PP-ZnO and Au/PT-ZnO is 0.80 and 0.83 wt%, respectively, and a similar Au loading can guarantee a feasible comparison between their gas-sensing performances.

### Gas-sensing measurement

Gas sensors were fabricated using PP-ZnO, PT-ZnO, Au/PP-ZnO and Au/PT-ZnO as sensing materials. These powder samples were mixed with ethanol to form pastes in an agate mortar. The paste was coated on a ceramic tube with a pair of Au electrodes and four Pt wires. After the ceramic tube coated with the sensing material was aged at 300 °C for 12 h in a muffle furnace, a Ni-Cr coil, as a heater to control the operation temperature by tuning the heating current, was inserted into the ceramic tube through the inner tube. Then both the ends of the Ni-Cr coil and the four Pt wires of the ceramic tube were melted to six electrodes of a pedestal to form a gas sensor, as shown in Fig. 1. The gas-sensing performances were tested using a CGS-8 gas sensor tester (Beijing Elite Technology Co., Ltd). As an n-type semiconductor, the response to the detected gas was defined as the ratio  $R_a/R_g$ , where  $R_a$  and  $R_g$  are the resistances in air and the detected gas, respectively. The experimental procedure is illustrated in Fig. 1.

### Cycle test

Acetone gas was injected into the gas chamber, and the resistance decreased. After the resistance value became stable, the air chamber was opened, and the resistance was gradually restored to the initial value. This step was repeated several times to test the stability of these samples.

### Dynamic sensing test

A certain amount of acetone was injected into the gas chamber to fix the concentration of acetone to 12.5 ppm, and the resistance decreased. After the resistance value became stable, a certain amount of acetone was injected into the gas chamber to fix the acetone concentration to 25 ppm. This step was repeated to test acetone with concentrations of 50, 100 and 200 ppm, and the dynamic sensing curves of these samples were obtained.

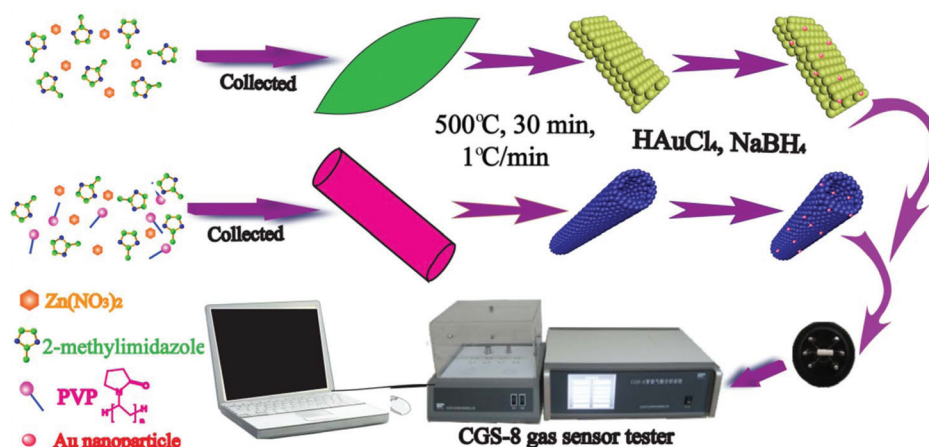


Fig. 1 Schematic illustration of the experimental procedure.

## Results and discussion

Zn(NO<sub>3</sub>)<sub>2</sub> can react with 2-MI in aqueous solution to form leaf-like ZIF-L (Fig. 2a and c),<sup>43,44</sup> while rod-like ZIF-L can be obtained with the aid of PVP (Fig. 2b and c).<sup>41</sup> The PXRD patterns of the two samples are identical, and all characteristic diffraction peaks correspond well to the simulated one,<sup>42</sup> which are comparable to those of the ZIF-L reported in the previous literature.<sup>45</sup>

Recently, hollow structure materials have drawn wide attention because of their excellent properties.<sup>46</sup> ZIFs, as a self-sacrificing template, possess some advantages like mild preparation conditions and simple operation.<sup>38,39</sup> The TGA results (as illustrated in Fig. 3a) reveal that both leaf-like ZIF-L and rod-like ZIF-L are almost decomposed sufficiently at *ca.* 500 °C. PXRD patterns reveal that ZnO can be obtained after ZIF-L is annealed at 500 °C (Fig. 3b).

As demonstrated in Fig. 4a–c, PP-ZnO derived from leaf-like ZIF-L exhibits a porous plate-like shape, not the leaf-like shape, indicating the destruction of the leaf-like ZIF-L after annealing at high temperature, while PT-ZnO derived from rod-like ZIF-L presents a porous tube structure (Fig. 4d–f). The wall of PT-ZnO consists of countless small particles, and the pores between the small particles will facilitate the diffusion and adsorption of the detected gas, leading to the improve-

ment of the gas-sensing performance. In addition, N<sub>2</sub> absorption–desorption isotherms, pore size distributions and the corresponding specific surface areas of the samples are shown in Fig. S1 and Table S1.† The hysteresis loops (Fig. S1a†) and pore size distributions (Fig. S1b†) reveal the existence of pores in these samples. However, the specific surface areas are small due to the large size of the samples.

When ZIF-L is annealed at high temperature (500 °C), 2-MI is thermally decomposed, resulting in the formation of an empty space originally occupied by 2-MI in ZIF-L, and Zn<sup>2+</sup> in ZIF-L reacts with the oxygen in air to form tiny ZnO particles which would agglomerate into larger particles to reduce the surface energy. For the rod-like ZIF-L, the decomposition of 2-MI would start from the outside of the rod-like ZIF-L, and then ZnO would be formed firstly at the outside of the rod-like ZIF-L to form a thin wall of the forthcoming tube-like structure. When 2-MI inside is decomposed, there is not enough oxygen to react with the Zn<sup>2+</sup> located at the inner part of the rod-like ZIF-L. Therefore, the Zn<sup>2+</sup> inside diffuses outward, finally leading to the formation of ZnO with a tube-like structure. As to the leaf-like ZIF-L, the decomposition of 2-MI would also start from the outside of the leaf-like ZIF-L. However, the thin thickness and large surface of the front side of the leaf-like ZIF-L do not facilitate the formation of a ZnO wall on the leaf-like ZIF-L, leading to the destruction of the leaf-like structure.

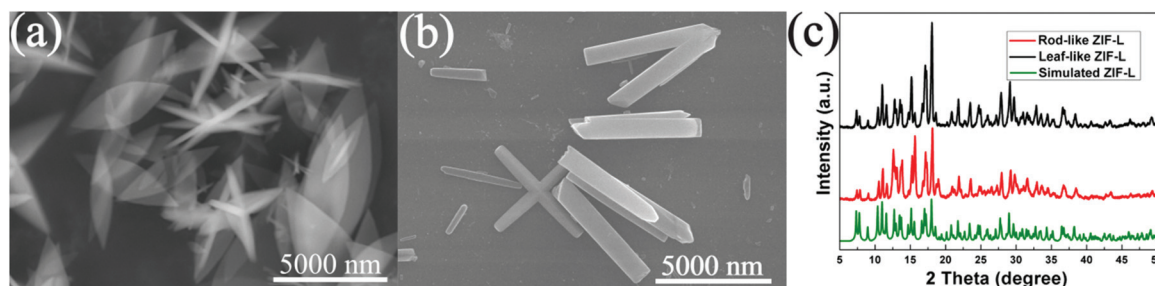


Fig. 2 SEM images of the (a) leaf-like and (b) rod-like ZIF-L. (c) PXRD patterns of the rod-like ZIF-L, leaf-like ZIF-L and simulated pattern of ZIF-L.<sup>42</sup>

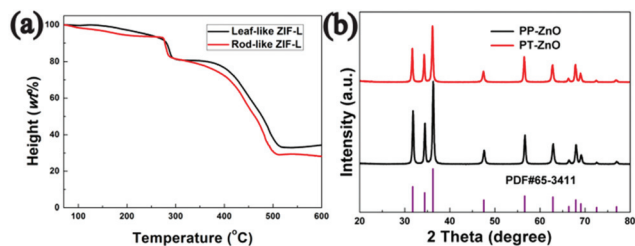


Fig. 3 (a) TG curves and (b) PXRD patterns of the leaf-like and rod-like ZIF-L.

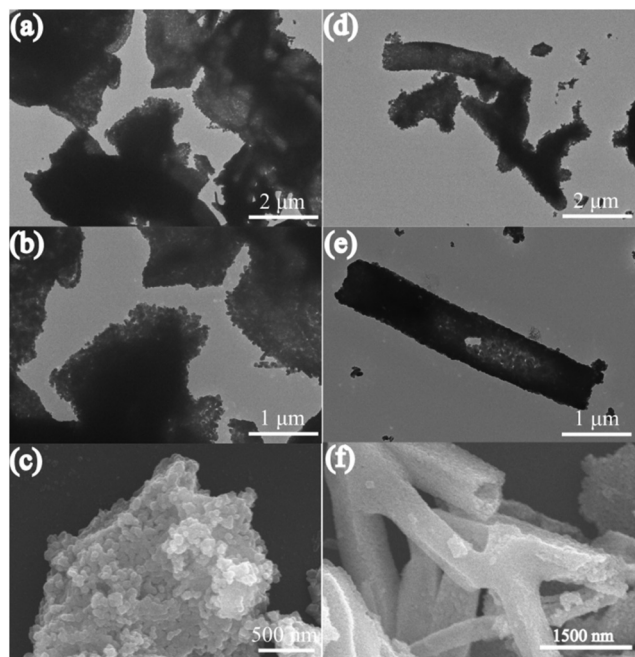


Fig. 4 TEM images of the (a, b) PP-ZnO and (d, e) PT-ZnO. SEM images of the (c) PP-ZnO and (f) PT-ZnO.

Loading with a noble metal on semiconductor oxide is generally considered an important method to improve the gas-sensing performance.<sup>47</sup> Therefore, Au NPs were introduced to achieve decoration using  $\text{HAuCl}_4$  and  $\text{NaBH}_4$ . Fig. 5a and b indicate that the Au NPs are loaded on the surface of the PT-ZnO successfully with the evidence of a weak PXRD diffraction peak at about  $38.2^\circ$  that can be assigned to the characteristic peak of Au NPs.<sup>48</sup> Because of the small size, low content of Au and high dispersion, the diffraction peaks of the Au NPs are weak. Furthermore, it can be seen from Fig. 5c and d that some tiny Au NPs exist on the surface of the PP-ZnO and PT-ZnO, in which the sizes of the Au NPs for the Au/PT-ZnO are smaller than those for the Au/PP-ZnO, indicating that the PT-ZnO is a good candidate to support Au NPs.

The gas-sensing performances of PP-ZnO, PT-ZnO, Au/PP-ZnO and Au/PT-ZnO were tested on a CGS-8 gas sensor tester. Acetone is detected by using the change of the resistance of the sensing material, and the response is defined as

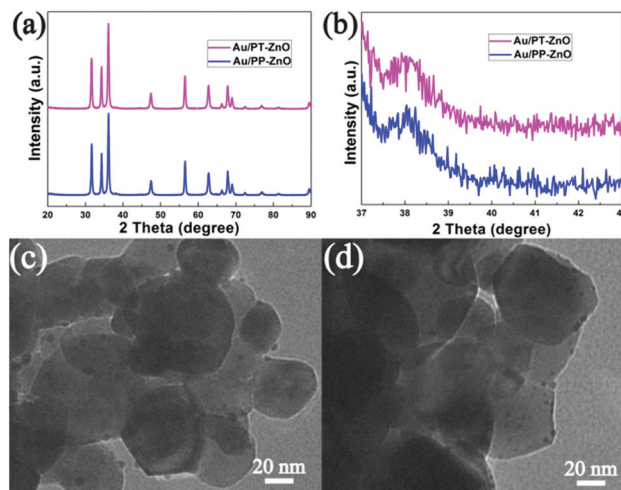


Fig. 5 (a, b) XRD patterns of the Au/PP-ZnO and Au/PT-ZnO and (c, d) TEM images of the (c) Au/PP-ZnO and (d) Au/PT-ZnO.

$R_a/R_g$ , in which  $R_a$  and  $R_g$  are the resistance of the sensing material in air and acetone, respectively. The responses of these four samples to 100 ppm acetone at different working temperatures were measured, as illustrated in Fig. 6a. It is shown that the response increases with the increase in the working temperature, and reaches the highest at  $210^\circ\text{C}$  for the PP-ZnO and PT-ZnO, and  $190^\circ\text{C}$  for the Au/PP-ZnO and Au/PT-ZnO, implying that the introduction of the Au NPs reduces the working temperature by  $20^\circ\text{C}$ . Subsequently, the responses decrease with a further increase in the working temperature. Acetone molecules are firstly adsorbed, then activated on the surface of the gas-sensing material, and finally reacted with the active oxygen species, leading to the change of resistance. When the working temperature is too low, the adsorbed acetone molecules cannot be activated sufficiently to react with the active oxygen species. When the working temperature is too high, the adsorbed acetone molecules will be desorbed from the surface of ZnO, resulting in the decrease of the response.

The responses of the PT-ZnO and PP-ZnO to 100 ppm acetone are 26 and 18, respectively. The higher response of the PT-ZnO can be probably attributed to the unique porous tube-like structure, which can facilitate the diffusion and adsorption of acetone molecules. The gas-sensing performance is improved greatly after Au NP loading, and the response of the Au/PT-ZnO is 280, that is, about 10 times higher than that of the pure PT-ZnO, which may be attributed to the larger amount of the active oxygen species and the activation of acetone by Au. Compared to the gas-sensing performance reported in the literature,<sup>49–57</sup> the Au/PT-ZnO exhibits a satisfactory response to acetone, as shown in Table S2.†

Fig. 6b exhibits that the responses increase with the increase in the concentration of acetone because the amount of acetone molecules adsorbed on the surface of the gas-sensing material increases gradually with the increase in the

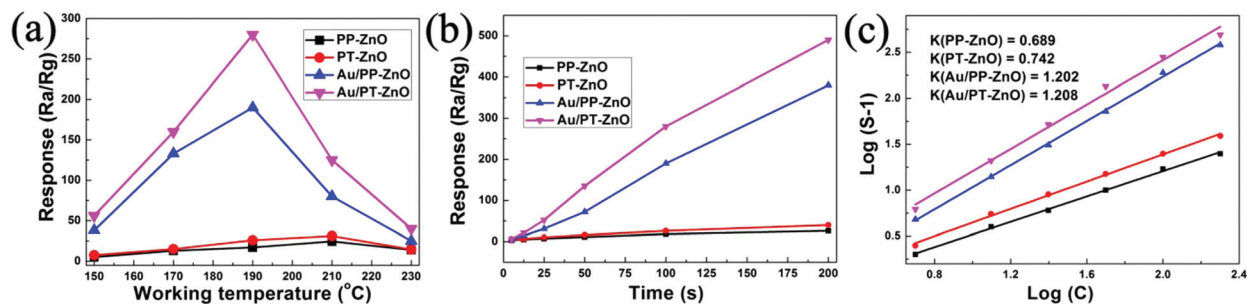


Fig. 6 (a) Response of the PP-ZnO, PT-ZnO and Au/PT-ZnO to 100 ppm acetone at different working temperatures, (b) response versus gas concentration curves of the samples in the range of 1–200 ppm and (c) the corresponding  $\log(S - 1)$  versus  $\log C$ .

concentration. The gas adsorption model of a semiconductor is empirically described as eqn (1):<sup>58</sup>

$$S = 1 + a(C)^b \quad (1)$$

where  $S$ ,  $C$ ,  $a$  and  $b$  are the sensitivity (or response), the concentration of the detected gas, a prefactor and an exponent on  $C$ , respectively. The value of  $b$  is usually 0.5 and 1, revealing that the active oxygen species is  $O^-$  and  $O^{2-}$ , respectively. Eqn (1) can be rewritten as eqn (2). It can be observed that there is a linear relationship between  $\log(S - 1)$  and  $\log C$ . As shown in Fig. 6c, the linear relationships are good for the PP-ZnO, PT-ZnO, Au/PP-ZnO and Au/PT-ZnO, and the values of the four samples are 0.689, 0.742, 1.202 and 1.208, respectively, indicating that the active oxygen species are  $O^-$  and  $O^{2-}$  for the former two samples, and mainly  $O^-$  for the latter two samples.

$$\log(S - 1) = a + b \log C. \quad (2)$$

The response–recovery curves by using resistance to different concentrations of acetone for PP-ZnO, PT-ZnO, Au/PP-ZnO and Au/PT-ZnO are shown in Fig. S3,† and the corresponding response time and recovery time are listed in Table S2.† It can be found that the responses to acetone with different concentrations are fast for all samples (lower than 20 s). When the concentration of acetone is low, the diffusion of the targeted gas to the surface of ZnO or Au/ZnO needs more time, and the corresponding response time is longer compared to the high acetone concentration. The recoveries are slow, and the recovery time increases with the increase in the acetone concentration, which may be due to the strong adsorption ability of acetone on the surface of these samples.

Fig. 7a shows the dynamic sensing curves of the PP-ZnO, PT-ZnO, Au/PP-ZnO and Au/PT-ZnO to different concentrations of acetone, and it is clearly seen that all the sensors exhibit excellent repeatability and stability. Fig. 7b exhibits that the response maintained relative stability without obvious changes even after six successive cycles, indicating the good stability and reproducibility of these samples. Additionally, selectivity is an important index to evaluate the gas-sensing performance. The responses to different gases, including acetone, ethanol, methanol, benzene, ammonia, hydrogen and carbon dioxide,

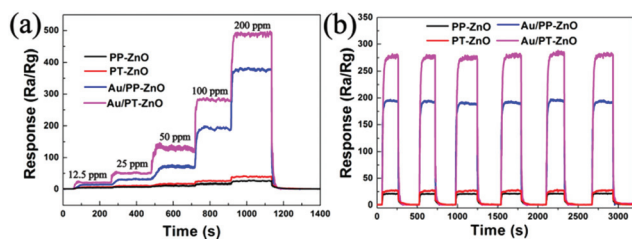


Fig. 7 (a) Dynamic sensing curves of the PP-ZnO, PT-ZnO, Au/PP-ZnO and Au/PT-ZnO to different concentrations of acetone and (b) cycle tests of the four samples to 100 ppm acetone.

were measured. It can be observed from Fig. 8 that the selectivity to acetone is satisfactory.

The most widely accepted sensing mechanism of semiconductor metal oxides is the depletion layer theory.<sup>59,60</sup> When ZnO, as an n-type semiconductor, is exposed to air, the  $O_2$  molecules in air will gain electrons from the conduction band of ZnO to form adsorbed oxygen ( $O_2^-$ ,  $O^-$  and  $O^{2-}$ ). Meanwhile, the resistance of ZnO increases and an electron depletion layer is formed on the surface of ZnO. When acetone is pumped in, acetone molecules are firstly adsorbed on the surface of ZnO and then reacted with the adsorbed oxygen, and electrons will be released to ZnO, leading to the decrease

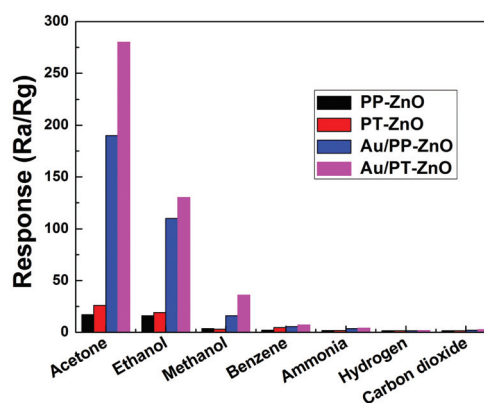


Fig. 8 Selectivity of the PP-ZnO, PT-ZnO, Au/PP-ZnO and Au/PT-ZnO to 100 ppm of different toxic gases.

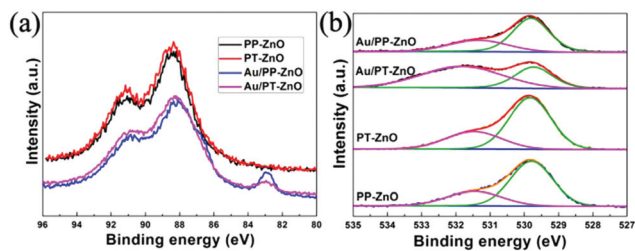


Fig. 9 (a) Zn 3p and Au 4f and (b) O 1s XPS spectra of the PP-ZnO, PT-ZnO, Au/PP-ZnO and Au/PT-ZnO.

of resistance and a thinner electron depletion layer. Therefore, the amount of adsorbed oxygen is of great importance for improving the gas-sensing performance, and a larger amount of adsorbed oxygen means better gas-sensing performance. To investigate the difference of the sensing properties, the XPS spectra were recorded, and the results are shown in Fig. 9 and Table S4.† Although part of the peaks of Au 4f<sub>5/2</sub> is overlapped by the signal of Zn 3p (Fig. 9a), the peak at about 83 eV proves the existence of Au for the Au-PP/ZnO and Au-PT/ZnO compared to the PP/ZnO and PT/ZnO. As shown in Fig. 9b, two peaks are obtained after peak fitting, and the peak at the low binding energy is assigned to the lattice oxygen (OI) of ZnO, while the peak at the high binding energy is assigned to adsorbed oxygen (OII) according to the previously published reports.<sup>61</sup> It can be observed that the percentages of OII onto the PP-ZnO and PT-ZnO are 29.0% and 30.5%, respectively. The higher percentage of OII onto the PT-ZnO implies better sensing performance than the PP-ZnO. In addition, the unique porous tube-like structure of the PT-ZnO facilitates the diffusion and adsorption of acetone molecules, which is good for improving the acetone-sensing performance.

Upon the introduction of Au NPs on the surface of the PP-ZnO and PT-ZnO, the percentages of OII are increased to 33.8% and 65.7%, respectively, which reveals that Au accelerates the formation of adsorbed oxygen and a thicker electron depletion layer. This is the reason why the acetone sensing performance of ZnO is improved after Au modification and the response of the Au/PT-ZnO is higher than that of the Au/PP-ZnO. It is worth noting that the OII becomes the dominant oxygen species for the Au/PT-ZnO, which may be assigned to the smaller size of the Au NPs compared to the Au/PP-ZnO. Furthermore, although the content of OII is not changed greatly for the PP-ZnO after the loading of Au NPs, the great improvement of the gas-sensing performance can also be attributed to the activation of acetone molecules by the Au NPs.

## Conclusions

In all, a facile preparation method of porous tube-like ZnO has been developed using rod-like ZIF-L as a self-sacrificing template. The response of the PT-ZnO to acetone is higher than that of the PP-ZnO derived from leaf-like ZIF-L, due to the

unique porous tube-like structure and larger amount of adsorbed oxygen. The acetone sensing performances are improved greatly after Au NP modification because of the activation of the acetone molecule by Au NPs and the increase of the adsorbed oxygen. In addition, the adsorbed oxygen becomes the dominant oxygen species for the Au/PT-ZnO because of the smaller size of Au NPs compared to the Au/PP-ZnO, resulting in the better acetone-sensing performance.

## Conflicts of interest

There are no conflicts to declare.

## Acknowledgements

This work was supported by the National Natural Science Foundation of China (21575011, 51578034), the Great Wall Scholars Training Program Project of Beijing Municipality Universities (CIT&TCD20180323), the Project of Construction of Innovation Teams and Teacher Career Development for Universities and Colleges Under Beijing Municipality (IDHT20170508), the Beijing Postdoctoral Research Foundation, the Beijing Talent Project (2017A38), and the Scientific Research Foundation of Beijing University of Civil Engineering and Architecture (KYJJ2017008).

## Notes and references

- 1 X. Pan, X. Liu, A. Bermak and Z. Fan, *ACS Nano*, 2013, 7, 9318.
- 2 S. Park, S. An, H. Ko, C. Jin and C. Lee, *ACS Appl. Mater. Interfaces*, 2012, 4, 3650.
- 3 W. W. Zhan, Q. Kuang, J. Z. Zhou, X. J. Kong, Z. X. Xie and L. S. Zheng, *J. Am. Chem. Soc.*, 2013, 135, 1926.
- 4 M. Drobek, J. H. Kim, M. Bechelany, C. Vallicari, A. Julbe and S. S. Kim, *ACS Appl. Mater. Interfaces*, 2016, 8, 8323.
- 5 M. Chen, Z. Wang, D. Han, F. Gu and G. Guo, *J. Phys. Chem. C*, 2011, 115, 12763.
- 6 Z. Wang, Z. Tian, D. Han and F. Gu, *ACS Appl. Mater. Interfaces*, 2016, 8, 5466.
- 7 J. Rao, A. Yu, C. Shao and X. Zhou, *ACS Appl. Mater. Interfaces*, 2012, 4, 5346.
- 8 X. Li, X. Zhou, H. Guo, C. Wang, J. Liu, P. Sun, F. Liu and G. Lu, *ACS Appl. Mater. Interfaces*, 2014, 6, 18661.
- 9 Z. Feng, Y. Ma, V. Natarajan, Q. Zhao, X. Ma and J. Zhan, *Sens. Actuators, B*, 2018, 255, 884.
- 10 Y. Zou, S. Chen, J. Sun, J. Liu, Y. Che, X. Liu, J. Zhang and D. Yang, *ACS Sens.*, 2017, 2, 897.
- 11 H. M. Jeong, J. H. Kim, S. Y. Jeong, C. H. Kwak and J. H. Lee, *ACS Appl. Mater. Interfaces*, 2016, 8, 7877.
- 12 B. Han, X. Liu, X. Xing, N. Chen, X. Xiao, S. Liu and Y. Wang, *Sens. Actuators, B*, 2016, 237, 423.
- 13 B. Han, X. Liu, X. Xing, N. Chen, X. Xiao, S. Liu and Y. Wang, *Sens. Actuators, B*, 2016, 237, 423.

- 14 J. H. Lee, *Sens. Actuators, B*, 2009, **140**, 319.
- 15 A. Katoch, Z. U. Abideen, J. H. Kim and S. S. Kim, *Sens. Actuators, B*, 2016, **232**, 698.
- 16 B. Y. Kim, Ju. S. Cho, J. W. Yoon, C. W. Na, C. S. Lee, J. H. Ahn, Y. C. Kang and J. H. Lee, *Sens. Actuators, B*, 2016, **234**, 353.
- 17 Z. Wang, H. Fu, Z. Tian, D. Han and F. Gu, *Nanoscale*, 2016, **8**, 5865.
- 18 Y. Liu, J. Goebel and Y. Yin, *Chem. Soc. Rev.*, 2013, **42**, 2610.
- 19 P. Rai, J. W. Yoon, H. M. Jeong, S. J. Hwang, C. H. Kwak and J. H. Lee, *Nanoscale*, 2014, **6**, 8292.
- 20 Z. Wen, Q. Wang and J. Li, *Adv. Funct. Mater.*, 2008, **18**, 959.
- 21 J. Y. Shen, L. Zhang, J. Ren, J. C. Wang, H. C. Yao and Z. J. Li, *Sens. Actuators, B*, 2017, **239**, 597.
- 22 N. Stock and S. Biswas, *Chem. Rev.*, 2012, **112**, 933.
- 23 J. Li, R. Kuppler and H. Zhou, *Chem. Soc. Rev.*, 2009, **38**, 1477.
- 24 Q. L. Zhu and Q. Xu, *Chem. Soc. Rev.*, 2014, **43**, 5468.
- 25 A. Schejcn, T. Mazet, V. Falk, L. Balan, L. Aranda, G. Medjahdi and R. Schneider, *Dalton Trans.*, 2015, **44**, 10136.
- 26 X. Wang, M. Li, C. Cao, C. Liu, J. Liu, Y. Zhu, S. Zhang and W. Song, *ChemCatChem*, 2016, **8**, 1.
- 27 H. P. Jing, C. C. Wang, Y. W. Zhang, R. Li and P. Wang, *RSC Adv.*, 2014, **4**, 54454.
- 28 Y. Zhang, Z. Xie, Z. Wang, X. Feng, Y. Wang and A. Wu, *Dalton Trans.*, 2016, **45**, 12653.
- 29 H. Bux, A. Feldhoff, J. Cravillon, M. Wiebcke, Y. S. Li and J. Caro, *Chem. Mater.*, 2011, **23**, 2262.
- 30 Q. Song, S. K. Nataraj, M. V. Roussanova, J. C. Tan, D. J. Hughes, W. Li, P. Bourgoïn, M. A. Alam, A. K. Cheetham, S. A. Al-Muhtasebd and E. Sivaniah, *Energy Environ. Sci.*, 2012, **5**, 8359.
- 31 B. Wang, A. P. Côté, H. Furukawa, M. O'Keeffe and O. M. Yaghi, *Nature*, 2008, **453**, 207.
- 32 H. Wu, W. Zhou and T. Yildirim, *J. Am. Chem. Soc.*, 2007, **129**, 5314.
- 33 Y. Hu, Z. Liu, J. Xu, Y. Huang and Y. Song, *J. Am. Chem. Soc.*, 2013, **135**, 9287.
- 34 P.-F. Liu, K. Tao, G.-C. Li, M.-K. Wu, S.-R. Zhu, F.-Y. Yi, W.-N. Zhao and L. Han, *Dalton Trans.*, 2016, **45**, 12632.
- 35 J. Yao and H. Wang, *Chem. Soc. Rev.*, 2014, **43**, 4470.
- 36 A. Zanon and F. Verpoort, *Coord. Chem. Rev.*, 2017, **353**, 201.
- 37 E. Chen, H. Yang and J. Zhang, *Inorg. Chem.*, 2014, **53**, 5411.
- 38 W. T. Koo, S. Yu, S. J. Choi, J. S. Jang, J. Y. Cheong and I. D. Kim, *ACS Appl. Mater. Interfaces*, 2017, **9**, 8201.
- 39 W. Li, X. Wu, H. Liu, J. Chen, W. Tang and Y. Chen, *New J. Chem.*, 2015, **39**, 7060.
- 40 V. K. Tomer, K. Singh, H. Kaur, M. Shorie and P. Sabherwal, *Sens. Actuators, B*, 2017, **253**, 703.
- 41 H. Fu, Z. Wang, X. Wang, P. Wang and C. C. Wang, *CrystEngComm*, 2018, **20**, 1473.
- 42 R. Chen, J. Yao, Q. Gu, S. Smeets, C. Baerlocher, H. Gu, D. Zhu, W. Morris, O. M. Yaghi and H. Wang, *Chem. Commun.*, 2013, **49**, 9500.
- 43 B. Motevalli, N. Taherifar, H. Wang and J. Z. Liu, *J. Phys. Chem. C*, 2017, **121**, 2221.
- 44 Z. Zhong, J. Yao, R. Chen, Z. Low, M. He, J. Z. Liu and H. Wang, *J. Mater. Chem. A*, 2015, **3**, 15715.
- 45 Z. X. Low, J. Yao, Q. Liu, M. He, Z. Wang, A. K. Suresh, J. Bellare and H. Wang, *Cryst. Growth Des.*, 2014, **14**, 6589.
- 46 J. Hu, M. Chen, X. Fang and L. Wu, *Chem. Soc. Rev.*, 2011, **40**, 5472.
- 47 X. W. Li, X. Zhou, H. Guo, C. Wang, J. Y. Liu, P. Sun, F. M. Liu and G. Lu, *ACS Appl. Mater. Interfaces*, 2014, **6**, 18661.
- 48 Y. Wei, Z. Zhao, X. Yu, B. Jin, J. Liu, C. Xu, A. Duan, G. Jiang and S. Ma, *Catal. Sci. Technol.*, 2013, **3**, 2958.
- 49 S. Kim, S. Park, S. Park and C. Lee, *Sens. Actuators, B*, 2015, **209**, 180.
- 50 Z. Feng, Y. Ma, V. Natarajan, Q. Zhao, X. Ma and J. Zhan, *Sens. Actuators, B*, 2018, **255**, 884.
- 51 L. Wang, Z. Lou, T. Fei and T. Zhang, *Sens. Actuators, B*, 2012, **161**, 178.
- 52 X. J. Wang, W. Wang and Y. L. Liu, *Sens. Actuators, B*, 2012, **168**, 39.
- 53 F. Li, T. Zhang, X. Gao, R. Wang and B. Li, *Sens. Actuators, B*, 2017, **252**, 822.
- 54 R. Xing, L. Xu, J. Song, C. Zhou, Q. Li, D. Liu and H. Song, *Sci. Rep.*, 2015, **5**, 10717.
- 55 X. Li, X. Zhou, H. Guo, C. Wang, J. Liu, P. Sun, F. Liu and G. Lu, *ACS Appl. Mater. Interfaces*, 2014, **6**, 18661.
- 56 J. Xia, K. Diao, Z. Zheng and X. Cui, *RSC Adv.*, 2017, **7**, 38444.
- 57 W. Li, X. Wu, N. Han, J. Chen, W. Tang and Y. Chen, *Powder Technol.*, 2016, **304**, 241.
- 58 Z. Wang, J. Xue, D. Han and F. Gu, *ACS Appl. Mater. Interfaces*, 2015, **7**, 308.
- 59 L. Zhang, R. Dong, Z. Zhu and S. Wang, *Sens. Actuators, B*, 2017, **245**, 112.
- 60 J. H. Kim, A. Mirzaei, H. W. Kim and S. S. Kim, *Sens. Actuators, B*, 2017, **249**, 177.
- 61 H. B. Huang, D. Y. C. Leung and D. Q. Ye, *J. Mater. Chem.*, 2011, **21**, 9647.